Letter

Hinge magnons from noncollinear magnetic order in a honeycomb antiferromagnet

Moon Jip Park,[1,2,*] SungBin Lee,[1,†] and Yong Baek Kim[3,‡]
[1]*Department of Physics, KAIST, Daejeon 34141, Republic of Korea*
[2]*Center of Theoretical Physics of Complex Systems, Institute for Basic Science, Daejeon 34126, Republic of Korea*
[3]*Department of Physics, University of Toronto, Toronto, Ontario, Canada M5S 1A7*

(Received 2 March 2021; revised 16 May 2021; accepted 22 July 2021; published 2 August 2021)

We propose that noncollinear magnetic order in magnetic systems can harbor a higher-order topological magnon phase with non-Hermitian topology and hinge magnon modes. We consider a three-dimensional system of interacting local moments on stacked layers of honeycomb lattice. It initially favors a collinear magnetic order along an in-plane direction, which turns into a noncollinear order upon applying an external magnetic field perpendicular to the easy axis. We exploit the non-Hermitian nature of the magnon Hamiltonian to show that this field-induced transition corresponds to the transformation from a topological magnon insulator to a higher-order topological magnon state with a one-dimensional hinge mode. As a concrete example, we discuss the recently discovered monoclinic phase of thin chromium trihalides, which we propose as a promising material candidate of the higher-order topological magnon phase.

DOI: 10.1103/PhysRevB.104.L060401

Introduction. Topological excitations in magnetic systems have emerged as novel platforms for potential applications in spintronics and quantum information technology [1]. A prominent recent path in pursuit of this direction is the research on topological phases of magnon excitations [2–8]. There has been an intense research effort to discover topological magnons in both gapless and gapped phases. Some examples of topological gapless excitations include the topological point and line-nodal magnons [3,9–14]. The candidate materials are $CrBr_3$ [9], $Cr_2Si_2Te_6$ [10], the three-dimensional Kitaev material β-Li_2IrO_3 [11], α-$RuCl_3$ [12], and the three-dimensional antiferromagnet Cu_3TeO_6 [13]. The gapped magnon spectrum may also carry nontrivial bulk topology, which physically manifests as the boundary magnon modes. The promising candidate materials are the layered transition metal trihalide CrI_3 [3] and the kagome magnet YMn_6Sn_6 [14].

The magnonic topological phases have often been understood in analogy with the counterparts of electronic topological systems. However, the topological magnons, in principle, may involve more complex physical phenomena, meaning that the electronic analogy may not be applicable. For example, topological magnons in noncollinear order are described by the intrinsically non-Hermitian Hamiltonian, which may lead to a variety of different topological phases [15–20]. In particular, such phases may support higher-order topological magnon phases, characterized by gapless $(d-2)$-dimensional boundary excitations in d-dimensional bulk [21–23].

In this work, we present a theoretical study of the magnonic higher-order topological excitations in noncollinear antiferromagnetic order. As a concrete example, we focus on a theoretical model relevant for the recently discovered monoclinic antiferromagnetic phase of thin chromium trihalides, CrI_3 [24–31] and $CrCl_3$ [31], where Cr local moments interact with each other in a three-dimensional system of stacked honeycomb lattices. It is shown that the external magnetic field perpendicular to the easy axis drives a phase transition from a collinear order to a noncollinear antiferromagnetic state [Fig. 1(b)], where the paraunitarity of the magnon wave function introduces the intrinsic non-Hermiticity in the magnon Hamiltonian [32,33]. In the noncollinear phase, it is shown that the simple analogy with electronic states does not apply. We find that the anomalous non-Hermitian terms in the model gap out the two-dimensional surface mode and generate a one-dimensional hinge magnon mode. Finally, we propose the symplectic Wilson loop as a bulk topological invariant that correctly captures the hinge magnon modes in higher-order topological magnon phases.

Spin model. A single layer of a chromium trihalide forms a simple honeycomb lattice of Cr atoms, which are surrounded by six adjacent nonmagnetic halide atoms. The multilayer monoclinic stacking (space group $C2/m$) is obtained by y-directional lateral shift to the neighboring layers [see Fig. 1(a)], which preserves the inversion, C_{2x} rotation, and their product, M_x, mirror symmetry. Motivated by recent experiments [24,31], we consider a minimal model for the interlayer antiferromagnetic order. The spin model consists of general intralayer and interlayer nearest-neighbor couplings that preserve the underlying symmetries of the $C2/m$ group:

$$H = \sum_{\langle i,j\rangle} J\mathbf{S}_i \cdot \mathbf{S}_j + \sum_{z_i = z_j + 1} J_\perp \mathbf{S}_i \cdot \mathbf{S}_j + \mathbf{D}_{\perp,ij} \cdot \mathbf{S}_i \times \mathbf{S}_j, \quad (1)$$

*moonjippark@ibs.re.kr
†sungbin@kaist.ac.kr
‡ybkim@physics.utoronto.ca

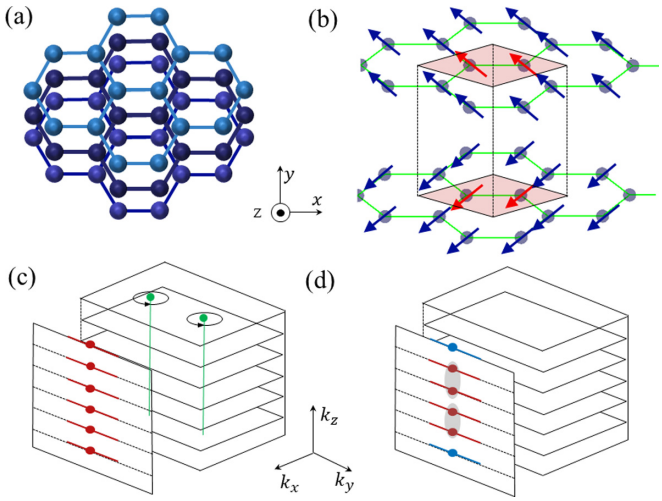

FIG. 1. (a) Top view of the atomic configurations in the monoclinic stacked honeycomb lattices. (b) Noncollinear magnetic order driven by an external magnetic field. Red spins represent the magnetic unit cell. (c) Locations of magnon zero modes in the Brillouin zone for the monoclinic structure, allowed by the spin-space group. Green points represent the nodal points protected by $\mathbb{Z}_2$-quantized Berry phase with the effective PT symmetry. The projection to the surface perpendicular to the x axis realizes the zigzag edge modes (red lines), which form an effective spin chain along the z direction (red dots). (d) In the noncollinear phase, the DMI dimerizes the edge modes in the effective Kitaev chain along the z direction, leaving only the hinge magnon states (blue lines).

where $J < 0$ and $J_\perp > 0$ represent the intralayer ferromagnetic and interlayer antiferromagnetic Heisenberg interactions, respectively. As long as the nearest-neighbor couplings are concerned, the inversion and C_{2x} symmetries allow only the interlayer Dzyaloshinskii-Moriya interaction (DMI), the direction of which lies on the y-z plane ($\mathbf{D}_\perp \perp \hat{\mathbf{x}}$), with the opposite signs for the two honeycomb sublattices (A and B). In addition, we assume the presence of single-ion anisotropy that stabilizes the antiferromagnetic order along an easy axis [34]. We note that our discussions of the hinge magnon excitation are not dependent on the anisotropy strength.

In the AA or rhombohedral (space group $R\bar{3}$) stacking, the additional C_{2y} and C_{3z} symmetries prohibit the interlayer DMI. The next-nearest-neighbor DMI appears as the next-leading-order coupling [3]. In such a case, each layer realizes the magnonic analog of the Haldane model, characterized by the nontrivial Chern number [4,5,35]. In this work, we focus on the symmetry-allowed nearest-neighbor interlayer couplings of the monoclinic stacking under the $C2/m$ group.

With a given magnetic ground state, the bosonic Bogoliubov–de Gennes (BdG) Hamiltonian can be derived by using the Holstein-Primakoff (HP) transformation [36]: $S_{+(-)} \approx \sqrt{2S}a^{(\dagger)}$, $S_z \approx S - a^\dagger a$, where the spin operators are expressed in the coordinates of the local ordered directions. The BdG Hamiltonian can be diagonalized via $H_{\mathrm{BdG}}(\mathbf{k}) = U_\mathbf{k} D_\mathbf{k} U_\mathbf{k}^\dagger$, where $D_\mathbf{k}$ is the diagonal matrix containing the magnon band energy. In the presence of the $U(1)$ spin rotation symmetry along the easy axis, the BdG Hamiltonian can be decoupled into two sectors as

$$H_{\mathrm{BdG}}(\mathbf{k}) = H_{s=+1} \oplus H_{s=-1}, \tag{2}$$

where each sector consists of the Hamiltonian of the magnons carrying spin ± 1 along the collinear axis. In this case, the wave functions satisfy the unitary condition, $U_\mathbf{k}^\dagger U_\mathbf{k} = I$, like the electron wave function does. However, in general noncollinear orders, the unitary condition is not satisfied. Instead, the bosonic commutation relation demands the paraunitary condition of the wave functions such that $U_\mathbf{k}^\dagger \Sigma_z U_\mathbf{k} = \Sigma_z$, where Σ_z is the Pauli matrix acting on the particle-hole space. Obtaining the paraunitary wave function requires the diagonalization of the non-Hermitian Hamiltonian $\Sigma_z H_{\mathrm{BdG}}(\mathbf{k})$ [37].

First-order topology in collinear order. When the spin-orbit coupling is negligibly small, the dominant interactions may approximately preserve symmetry operations higher than is strictly required by the magnetic space group. The set of these operations is formally referred to as the spin-space group [38,39]. The spin-space group consists of larger rotational symmetries than that of the magnetic space group [40], which independently act on the coordinate rotations and the spin rotations. Therefore, under the spin-space group, we can define the effective space-time inversion symmetry PT, which provides the topological protection of the $\mathbb{Z}_2$-quantized Berry phase along a closed loop in the Brillouin zone (BZ) [41,42].

Without the interlayer interactions, each layer possesses the Dirac nodal points at the K and K' points [see Fig. 1(c)]. The topological protection of the nodal point can be formally cast by the $\mathbb{Z}_2$-quantized Berry phase π along a loop encircling the nodal points [black circles in Fig. 1(c)]. The physical manifestation of the π Berry phase is the zigzag edge modes, like in monolayer graphene [43]. The π Berry phase is still well defined in the presence of the interlayer coupling along a loop encircling the nodal line in the three-dimensional BZ. It manifests as the two-dimensional flat band on the surface of the three-dimensional bulk [44,45]. This first-order topological surface state has been similarly considered in the context of bulk graphite [46,47]. In the presence of non-negligible spin-orbit coupling, DMI may open a band gap, leading to the magnonic topological insulator with a nontrivial Chern number [3].

Second-order topology in noncollinear order. We now consider the external magnetic field along the direction perpendicular to the collinear antiferromagnetic order. That is, we add the term $H_{\mathrm{ext}} = -\mathbf{h}_{\mathrm{ext}} \cdot \sum_i \mathbf{S}_i$, where $\mathbf{h}_{\mathrm{ext}}$ represents the external magnetic field. The magnetic field generates the noncollinear order with the spin canting [see Fig. 1(b)]. In this case, the conventional Wilson line and the Berry phase are not well defined anymore since the wave function does not satisfy the unitary condition [37]. Instead, we show that the noncollinearity induced by the spin canting generates the higher-order topological hinge magnon states [see Fig. 1(d)].

As an example, we first consider the specific case where the x-directional magnetic field is applied to the y-directional antiferromagnetic order. Figure 2(a) shows the noncollinear magnon bands. We find that the zigzag edge modes at the surface are immediately gapped out as the magnetic field is applied [inset in Fig. 2(a)]. In contrast, a pair of in-gap states emerges within the momentum window $K < k_y < K'$ [red dashed line in Fig. 2(a)], as we take the additional open

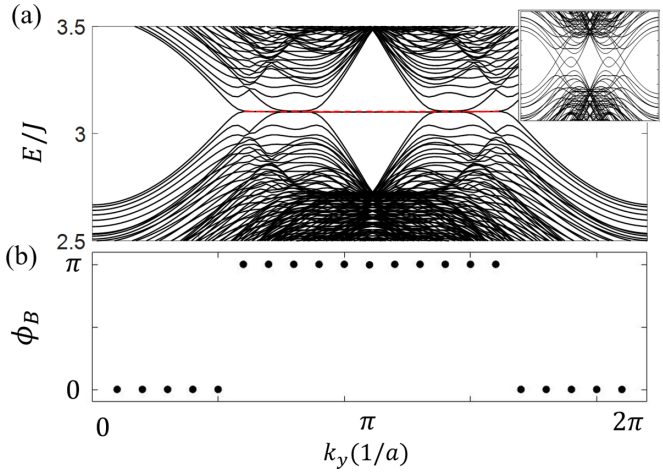

FIG. 2. (a) The magnon band structure as a function of k_y with the open boundary condition along the x-z direction. In the middle of the bands, the hinge magnon states emerge (red line). Inset: the same band structure with the periodic boundary condition along the z direction. Here, the DM vector is pointing in the z direction. (b) The non-Abelian Berry phase as a function of k_y. We find the π-quantized Berry phase at k_y, where the hinge modes reside.

boundary condition along the z direction. Unlike the surface states, these in-gap states are localized at the corner of the x-z plane, evidently showing the nature of the hinge modes (Fig. 3). In addition, unlike the conventional electronic higher-order topological insulators, the localization of the hinge modes occurs only at the two corners of one side surface. The surface possessing the hinge mode switches as the direction of the magnetic field is inverted.

Effective surface model. A heuristic way of understanding the emergence of the hinge state is to consider the effective model describing the zigzag edge modes at the surface [Fig. 4(a)]. At a fixed k_y, we can consider the zigzag edges as the effective one-dimensional antiferromagnetic chain

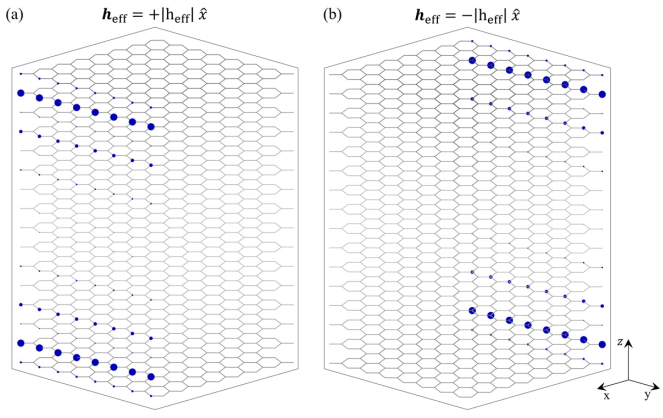

FIG. 3. The wave function of the hinge modes. We find that the wave functions are localized at one of the corners of the x-z plane, depending on the direction of the field. The magnetic field is applied along the (a) $+\hat{x}$ and (b) $-\hat{x}$ directions. The periodic boundary condition is imposed along the $\hat{y}$ direction. The size of the blue dot indicates the amplitude of the wave functions.

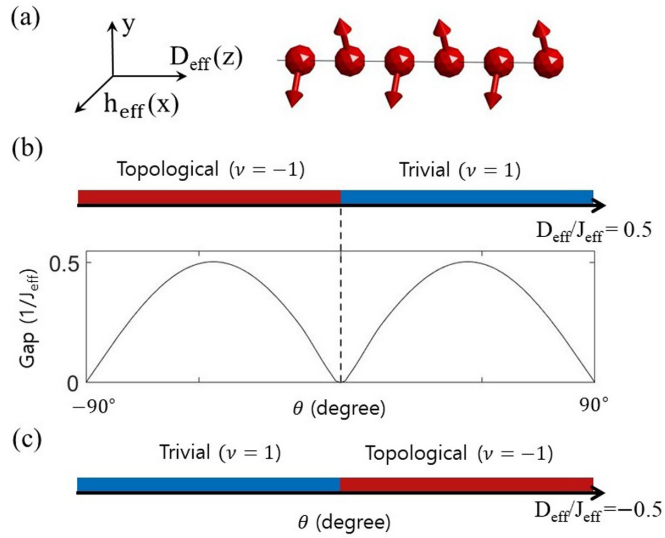

FIG. 4. (a) Schematic picture of the one-dimensional spin chain along the $\hat{z}$ direction. The external magnetic field is applied along the $\hat{x}$ direction, while the DM vector is pointing in the $\hat{z}$ direction. (b) The band gap and topological phase diagram as a function of the external magnetic field and the DMI. The topological phase (red strip) is characterized by the topological number $\nu = -1$ (π Berry phase). The physical manifestation is the zero-dimensional bound mode at the end of the chain. (c) The same phase diagram as in (b), but the direction of the DMI is reversed.

($J_{\rm eff} > 0$) along the $\hat{z}$ direction,

$$H_{\rm eff} = \sum_{\langle i,j\rangle} J_{\rm eff}\mathbf{S}_i \cdot \mathbf{S}_j + (D_{\rm eff}\hat{z}) \cdot \mathbf{S}_i \times \mathbf{S}_j - (h_{\rm eff}\hat{x}) \cdot \sum_i \mathbf{S}_i, \tag{3}$$

where the subscript index i indicates the ith layer. The noncollinear order in the presence of the spin canting can be represented with the cant angle θ as $\vec{S}_i = |S|(\sin\theta, (-1)^i\cos\theta, 0)$. Due to the noncollinearity, the HP transformations of the Heisenberg exchange interaction and the DMI now contain both particle-particle and particle-hole channels as

$$\begin{aligned} J_{\rm eff} &: \mathbf{S}_{i+1} \cdot \mathbf{S}_i \\ &= \frac{|S|}{2}[\sin^2\theta a^\dagger_{i+1}a_i - \cos^2\theta a^\dagger_{i+1}a^\dagger_i - n_{i+1} - n_i] + \text{H.c.}, \end{aligned}$$

$$\begin{aligned} D_{\rm eff} &: \hat{z} \cdot \mathbf{S}_{i+1} \times \mathbf{S}_i \\ &= \frac{|S|}{2}\left[\frac{(-1)^i}{2}\sin 2\theta(a^\dagger_{i+1}a_i + a^\dagger_{i+1}a^\dagger_i - n_{i+1} - n_i)\right] + \text{H.c.}, \end{aligned} \tag{4}$$

where n_i is the HP boson number operator. Here, we have collected only the quadratic terms of the HP bosons within the linear spin-wave theory. The resulting HP Hamiltonian consists of the normal hopping and p-wave pairing terms as well as a chemical potential and resembles the Kitaev chain model [48] that possesses the Majorana fermions at the boundary.

We now formally show that the above one-dimensional spin chain is characterized by the nontrivial topology. By

collecting the interactions in Eq. (4), we derive the full tight-binding model of the HP bosons as

$$H_{\mathrm{HP}} = \frac{|S|}{2}\sum_i t_{\mathrm{eff},i}[a_{i+1}^\dagger a_i + a_{i+1}a_i^\dagger] + \Delta_{\mathrm{eff},i}[a_{i+1}^\dagger a_i^\dagger + a_{i+1}a_i] - \mu_{\mathrm{eff}}[a_i^\dagger a_i + a_i a_i^\dagger] + \mathrm{H.c.}, \tag{5}$$

where the explicit forms of the coupling parameters are given by

$$t_{\mathrm{eff},i} = \frac{J_{\mathrm{eff}}}{2}(1-\cos 2\theta) + (-1)^i\frac{D_{\mathrm{eff}}}{2}\sin 2\theta,$$
$$\Delta_{\mathrm{eff},i} = -\frac{J_{\mathrm{eff}}}{2}(1+\cos 2\theta) + (-1)^i\frac{D_{\mathrm{eff}}}{2}\sin 2\theta,$$
$$\mu_{\mathrm{eff}} = -2J_{\mathrm{eff}}\cos 2\theta - \frac{h_{\mathrm{eff}}}{|S|}\sin\theta. \tag{6}$$

The above Hamiltonian can be analytically diagonalized (see the Supplemental Material [49]). Indeed, we find that it supports two topologically distinct gapped phases: the nontrivial phase with the zero-dimensional boundary mode and the trivial gapped phase. The topological phase transition between the two gapped phases occurs when $\theta = 0$, regardless of the specific parameters in the HP Hamiltonian [Fig. 4(b)]. This behavior explains the emergence of the hinge mode even with an arbitrarily small strength of the magnetic field. By further increasing the strength of the magnetic field, we find that the magnon band gap closes at the cant angle $\theta = \pm 90^\circ$, where the system regains the collinearity along the direction of the magnetic field.

Furthermore, the nontrivial phase is determined by the relative orientation between the Dzyaloshinskii-Moriya (DM) vector and the direction of the magnetic field [Fig. 4(c)]. In the full three-dimensional model, the zigzag edges of the two side surfaces consist of different sublattices, in which the directions of the DMIs are reversed from each other. Therefore, at a given direction of the magnetic field, one of the two side surfaces becomes topologically nontrivial, while the other surface is topologically trivial. As a result, only two hinge modes occur at one of the side surfaces, which explains the localization pattern of the hinge mode in the three-dimensional model (Fig. 3). Finally, we note that our results hold regardless of the specific direction of the collinear magnetic order as long as the external magnetic field is applied in the perpendicular direction. As we show next, the hinge modes are robust as long as the magnetic order preserves C_{2x} symmetry. In general, C_{2x} symmetry can be broken by the addition of the random disorder. The effect of the disorder is examined by adding the Anderson-type disorder to the HP Hamiltonian. We find that the localization of the hinge modes at the corner survives well even when the disorder strength well exceeds the size of the band gap. (See the Supplemental Material for the detailed implementation.)

Symplectic Wilson loop. To rigorously describe the topology of the paraunitary wave functions, we introduce the topological invariant. The particle-hole symmetry of the BdG Hamiltonian allows the decomposition of the wave functions into the positive- and negative-energy sectors as $U_{\mathbf{k}} = (V_{\mathbf{k}}, \Sigma_x V_{-\mathbf{k}})$, where $V_{\mathbf{k}}$ is an $(N \times \frac{N}{2})$-dimensional matrix, containing the eigenvectors of the positive-energy sector [12,50,51]. The wave functions of the positive-energy sectors satisfy the following normalization condition: $V_{\mathbf{k}}^\dagger \Sigma_z V_{\mathbf{k}} = I$. Using this property, we can define the *symplectic Wilson line* as

$$\mathcal{U}_s(\boldsymbol{k}_1 \to \boldsymbol{k}_2) \equiv \Sigma_z \hat{P}(\boldsymbol{k}_1)\left[\prod_{\boldsymbol{k}} \Sigma_z \hat{P}(\boldsymbol{k})\right]\Sigma_z \hat{P}(\boldsymbol{k}_2), \tag{7}$$

where the momentum vectors $\mathbf{k}$ form a path from $\boldsymbol{k}_1$ to $\boldsymbol{k}_2$. $[\hat{P}(\boldsymbol{k})]_{ij} = \sum_{n\in\mathrm{occupied}}[V_{\mathbf{k}}]_{i,n}[V_{\mathbf{k}}^\dagger]_{n,j}$ is the projection operator to the occupied positive-energy subspace at the momentum $\boldsymbol{k}$. The Wilson line measures the non-Abelian Berry phase as the eigenstates adiabatically shift momentum from k_1 to k_2, and it becomes a gauge-invariant quantity as the line forms a loop in the Brillouin zone. In contrast to the conventional Wilson line, the additional operator Σ_z is inserted between the projection operators. It is important to note that Eq. (7) along a closed loop recovers the unitarity due to the normalization condition. Utilizing the unitarity condition, we can formally define the non-Abelian Berry phase of the paraunitary wave functions as

$$e^{i\Phi_{\mathrm{B}}(\boldsymbol{k}_1\to\boldsymbol{k}_2)} = \det[\mathcal{U}_s(\boldsymbol{k}_1 \to \boldsymbol{k}_2)\Sigma_z]. \tag{8}$$

In general, the Berry phase can be any arbitrary value between zero and 2π ($\Phi_{\mathrm{B}} \in [0, 2\pi)$). However, in the presence of C_{2x} rotation symmetry, the Berry phase becomes quantized. To show this, we consider the one-dimensional Hamiltonian shown above. We now introduce the topological invariant ν. Using C_{2x} symmetry, we can decompose the Wilson loop into the two Wilson lines related by C_{2x} symmetry as

$$\begin{aligned}\nu \equiv e^{i\Phi_B} &= \det[\mathcal{U}_{s,(0\to\pi)}\mathcal{U}_{s,(\pi\to 2\pi)}\Sigma_z] \\ &= \det\left[\mathcal{U}_{s,(0\to\pi)}\hat{C}_{2x}^{-1}\left(\hat{C}_{2x}\mathcal{U}_{s,(\pi\to 2\pi)}\hat{C}_{2x}^{-1}\right)\hat{C}_{2x}\Sigma_z\right] \\ &= \det\left[\mathcal{U}_{s,(0\to\pi)}\hat{C}_{2x}^{-1}\mathcal{U}_{s,(\pi\to 0)}\hat{C}_{2x}\Sigma_z\right] \\ &= \prod_{n\in\mathrm{occupied}} \zeta_n(0)\zeta_n(\pi),\end{aligned} \tag{9}$$

where $\zeta_n(k)$ is the eigenvalue of C_{2x} on the nth band at momentum k. Since $\zeta_n = \pm 1$ ($C_{2x}^2 = 1$), the Berry phase can only be zero or π, which gives rise to $\mathbb{Z}_2$-topological protection of the hinge mode. (See the Supplemental Material for the detailed mathematical proof.)

We now numerically calculate the Wilson loop via integration along the k_z direction in the three-dimensional model with the open boundary condition in the x direction. Figure 2(b) shows the computed Berry phase as a function of k_y. We find the quantized π Berry phase at C_{2x}-invariant momentum, $k_y = \pi$, where the hinge modes appear ($K < k_y < K'$). The π-quantized Berry phase signals the boundary modes in the x-z plane [52,53], which physically manifest as the hinge mode. We also note that the higher-order topological invariant is characterized by the two-dimensional bulk at fixed momenta k_y. As a result, the hinge mode is realized as the corner modes at fixed transverse momentum k_y, which is similar to the hinge-arc states observed in higher-order topological semimetals [54]

Discussion. In conclusion, we have proposed a theoretical model for the higher-order topological hinge magnon excitations in the three-dimensional system of layered honeycomb

antiferromagnets. It was shown that the magnetic-field-driven phase transition from a collinear magnetic order to a noncollinear magnetic order corresponds to the topological phase transition from a magnon topological insulator to a high-order topological magnon state with hinge magnon modes. We showed that the non-Hermitian nature of the magnon Hamiltonian and the paraunitarity of the magnon wave function play crucial roles here. While the conventional Wilson loop approach fails to capture the topology of the system, we demonstrated that the symplectic Wilson loop method offers an alternative topological invariant. Our results suggest that the external magnetic field can be used as a control knob for the topological phase transition.

We proposed the multilayer chromium trihalides as a promising material candidate of the higher-order topological magnon phase. A recent Raman spectroscopy measurement identified the presence of the monoclinic phase ($C2/m$) in thin multilayers of CrI_3 [24] and $CrCl_3$ [31]. The interlayer antiferromagnetism was further confirmed through magneto-optical Kerr effect measurement [26,27] and tunneling magnetoresistance [28–30], which is consistent with the magnetic ordering pattern in our theoretical model. We may also expect a sizable strength of DMI as in the bulk sample. We have shown that the interlayer stacking order plays a crucial role in the form of the DMI and the higher-order topology. Experimentally, the monoclinic phases are stable in the thin film, while the bulk sample undergoes the structural phase transition to the rhombohedral structure ($R\bar{3}$) [25]. Therefore, investigations of magnetic properties by varying the layer thickness would reveal an interesting interplay between the stacking order and topology. In addition, we also suggest that an external electric field could be used to control the interlayer DMI [55–57]. In particular, an electric field along the x direction would generate the interlayer DMI by breaking C_{2y} symmetry even in the rhombohedral structure ($R\bar{3}$).

Finally, it is worthwhile to mention that the family of A_2MO_3 compounds (A = Na, Li; M = transition metal) also contains many monoclinic honeycomb antiferromagnets [58–62]. A zigzag in-plane order in addition to the interlayer antiferromagnetism has been observed in these materials. In such a case, the additional zone folding occurs along the in-plane directions. The effect of the additional in-plane order on the topology would be an interesting subject of future study.

Acknowledgments. The numerical calculations of the linear spin-wave theory were performed using the SPINW software program [63]. M.J.P. and S.L. are supported by the National Research Foundation Grant (Grants No. NRF-2020R1F1A1073870 and No. NRF- 2020R1A4A3079707). Y.B.K. is supported by NSERC of Canada and the Center for Quantum Materials at the University of Toronto. M.J.P. is supported by the Institute for Basic Science of Korea (Grant No. IBS-R024-D1).

[1] A. V. Chumak, V. I. Vasyuchka, A. A. Serga, and B. Hillebrands, Magnon spintronics, Nat. Phys. **11**, 453 (2015).
[2] H. Katsura, N. Nagaosa, and P. A. Lee, Theory of the Thermal Hall Effect in Quantum Magnets, Phys. Rev. Lett. **104**, 066403 (2010).
[3] L. Chen, J.-H. Chung, B. Gao, T. Chen, M. B. Stone, A. I. Kolesnikov, Q. Huang, and P. Dai, Topological Spin Excitations in Honeycomb Ferromagnet CrI_3, Phys. Rev. X **8**, 041028 (2018).
[4] S. A. Owerre, A first theoretical realization of honeycomb topological magnon insulator, J. Phys.: Condens. Matter **28**, 386001 (2016).
[5] S. A. Owerre, Topological honeycomb magnon Hall effect: A calculation of thermal Hall conductivity of magnetic spin excitations, J. Appl. Phys. **120**, 043903 (2016).
[6] H. Kondo, Y. Akagi, and H. Katsura, Three-dimensional topological magnon systems, Phys. Rev. B **100**, 144401 (2019).
[7] A. Mook, K. Plekhanov, J. Klinovaja, and D. Loss, Interaction-Stabilized Topological Magnon Insulator in Ferromagnets, Phys. Rev. X **11**, 021061 (2021).
[8] R. Shindou, R. Matsumoto, S. Murakami, and J.-i. Ohe, Topological chiral magnonic edge mode in a magnonic crystal, Phys. Rev. B **87**, 174427 (2013).
[9] E. J. Samuelsen, R. Silberglitt, G. Shirane, and J. P. Remeika, Spin waves in ferromagnetic $CrBr_3$ studied by inelastic neutron scattering, Phys. Rev. B **3**, 157 (1971).
[10] T. J. Williams, A. A. Aczel, M. D. Lumsden, S. E. Nagler, M. B. Stone, J.-Q. Yan, and D. Mandrus, Magnetic correlations in the quasi-two-dimensional semiconducting ferromagnet $CrSiTe_3$, Phys. Rev. B **92**, 144404 (2015).
[11] W. Choi, T. Mizoguchi, and Y. B. Kim, Nonsymmorphic-Symmetry-Protected Topological Magnons in Three-Dimensional Kitaev Materials, Phys. Rev. Lett. **123**, 227202 (2019).
[12] F. Lu and Y.-M. Lu, Magnon band topology in spin-orbital coupled magnets: Classification and application to α-$RuCl_3$, arXiv:1807.05232.
[13] K. Li, C. Li, J. Hu, Y. Li, and C. Fang, Dirac and Nodal Line Magnons in Three-Dimensional Antiferromagnets, Phys. Rev. Lett. **119**, 247202 (2017).
[14] H. Zhang, X. Feng, T. Heitmann, A. I. Kolesnikov, M. B. Stone, Y.-M. Lu, and X. Ke, Topological magnon bands in a room-temperature kagome magnet, Phys. Rev. B **101**, 100405(R) (2020).
[15] H. Shen, B. Zhen, and L. Fu, Topological Band Theory for Non-Hermitian Hamiltonians, Phys. Rev. Lett. **120**, 146402 (2018).
[16] T. Liu, Y.-R. Zhang, Q. Ai, Z. Gong, K. Kawabata, M. Ueda, and F. Nori, Second-Order Topological Phases in Non-Hermitian Systems, Phys. Rev. Lett. **122**, 076801 (2019).
[17] N. Okuma, K. Kawabata, K. Shiozaki, and M. Sato, Topological Origin of Non-Hermitian Skin Effects, Phys. Rev. Lett. **124**, 086801 (2020).
[18] M. S. Rudner and L. S. Levitov, Topological Transition in a Non-Hermitian Quantum Walk, Phys. Rev. Lett. **102**, 065703 (2009).
[19] S. Yao and Z. Wang, Edge States and Topological Invariants of Non-Hermitian Systems, Phys. Rev. Lett. **121**, 086803 (2018).
[20] M. Ezawa, Non-Hermitian higher-order topological states in nonreciprocal and reciprocal systems with their electric-circuit realization, Phys. Rev. B **99**, 201411(R) (2019).

[21] A. Mook, S. A. Díaz, J. Klinovaja, and D. Loss, Chiral hinge magnons in second-order topological magnon insulators, Phys. Rev. B **104**, 024406 (2021).

[22] A. Sil and A. K. Ghosh, First and second order topological phases on ferromagnetic breathing kagome lattice, J. Phys.: Condens. Matter **32**, 205601 (2020).

[23] T. Hirosawa, S. A. Díaz, J. Klinovaja, and D. Loss, Magnonic Quadrupole Topological Insulator in Antiskyrmion Crystals, Phys. Rev. Lett. **125**, 207204 (2020).

[24] N. Ubrig, Z. Wang, J. Teyssier, T. Taniguchi, K. Watanabe, E. Giannini, A. F. Morpurgo, and M. Gibertini, Low-temperature monoclinic layer stacking in atomically thin CrI_3 crystals, 2D Mater. **7**, 015007 (2019).

[25] M. A. McGuire, H. Dixit, V. R. Cooper, and B. C. Sales, Coupling of crystal structure and magnetism in the layered, ferromagnetic insulator CrI_3, Chem. Mater. **27**, 612 (2015).

[26] T. Song, X. Cai, M. W.-Y. Tu, X. Zhang, B. Huang, N. P. Wilson, K. L. Seyler, L. Zhu, T. Taniguchi, K. Watanabe, M. A. McGuire, D. H. Cobden, D. Xiao, W. Yao, and X. Xu, Giant tunneling magnetoresistance in spin-filter van der Waals heterostructures, Science **360**, 1214 (2018).

[27] B. Huang, G. Clark, E. Navarro-Moratalla, D. R. Klein, R. Cheng, K. L. Seyler, D. Zhong, E. Schmidgall, M. A. McGuire, D. H. Cobden, W. Yao, D. Xiao, P. Jarillo-Herrero, and X. Xu, Layer-dependent ferromagnetism in a van der Waals crystal down to the monolayer limit, Nature (London) **546**, 270 (2017).

[28] D. R. Klein, D. MacNeill, J. L. Lado, D. Soriano, E. Navarro-Moratalla, K. Watanabe, T. Taniguchi, S. Manni, P. Canfield, J. Fernández-Rossier, and P. Jarillo-Herrero, Probing magnetism in 2D van der Waals crystalline insulators via electron tunneling, Science **360**, 1218 (2018).

[29] Z. Wang, I. Gutiérrez-Lezama, N. Ubrig, M. Kroner, M. Gibertini, T. Taniguchi, K. Watanabe, A. Imamoğlu, E. Giannini, and A. F. Morpurgo, Very large tunneling magnetoresistance in layered magnetic semiconductor CrI_3, Nat. Commun. **9**, 2516 (2018).

[30] H. H. Kim, B. Yang, T. Patel, F. Sfigakis, C. Li, S. Tian, H. Lei, and A. W. Tsen, One million percent tunnel magnetoresistance in a magnetic van der Waals heterostructure, Nano Lett. **18**, 4885 (2018).

[31] D. R. Klein, D. MacNeill, Q. Song, D. T. Larson, S. Fang, M. Xu, R. A. Ribeiro, P. C. Canfield, E. Kaxiras, R. Comin, and P. Jarillo-Herrero, Enhancement of interlayer exchange in an ultrathin two-dimensional magnet, Nat. Phys. **15**, 1255 (2019).

[32] P. A. McClarty and J. G. Rau, Non-Hermitian topology of spontaneous magnon decay, Phys. Rev. B **100**, 100405(R) (2019).

[33] J. G. Rau, R. Moessner, and P. A. McClarty, Magnon interactions in the frustrated pyrochlore ferromagnet $Yb_2Ti_2O_7$, Phys. Rev. B **100**, 104423 (2019).

[34] A. McLachlan, Spin-spin coupling Hamiltonian in spin multiplets, Mol. Phys. **6**, 441 (1963).

[35] F. D. M. Haldane, Model for a Quantum Hall Effect without Landau Levels: Condensed-Matter Realization of the "Parity Anomaly," Phys. Rev. Lett. **61**, 2015 (1988).

[36] T. Holstein and H. Primakoff, Field dependence of the intrinsic domain magnetization of a ferromagnet, Phys. Rev. **58**, 1098 (1940).

[37] J. Colpa, Diagonalization of the quadratic boson hamiltonian, Phys. A (Amsterdam, Neth.) **93**, 327 (1978).

[38] W. F. Brinkman and R. J. Elliott, Theory of spin-space groups, Proc. R. Soc. London, Ser. A **294**, 343 (1966).

[39] W. Brinkman and R. J. Elliott, Space group theory for spin waves, J. Appl. Phys. **37**, 1457 (1966).

[40] J. Zak, Magnetic translation group, Phys. Rev. **134**, A1602 (1964).

[41] J. C. Y. Teo and C. L. Kane, Topological defects and gapless modes in insulators and superconductors, Phys. Rev. B **82**, 115120 (2010).

[42] S. Ryu, A. P. Schnyder, A. Furusaki, and A. W. W. Ludwig, Topological insulators and superconductors: Tenfold way and dimensional hierarchy, New J. Phys. **12**, 065010 (2010).

[43] M. Fujita, K. Wakabayashi, K. Nakada, and K. Kusakabe, Peculiar localized state at zigzag graphite edge, J. Phys. Soc. Jpn. **65**, 1920 (1996).

[44] K.-K. Li and J.-P. Hu, Weyl and nodal ring magnons in three-dimensional honeycomb lattices, Chin. Phys. Lett. **34**, 077501 (2017).

[45] G. Bian, T.-R. Chang, H. Zheng, S. Velury, S.-Y. Xu, T. Neupert, C.-K. Chiu, S.-M. Huang, D. S. Sanchez, I. Belopolski, N. Alidoust, P.-J. Chen, G. Chang, A. Bansil, H.-T. Jeng, H. Lin, and M. Z. Hasan, Drumhead surface states and topological nodal-line fermions in $TlTaSe_2$, Phys. Rev. B **93**, 121113(R) (2016).

[46] G. E. Volovik and V. M. Pudalov, Graphite on graphite, JETP Lett. **104**, 880 (2016).

[47] T. T. Heikkilä and G. E. Volovik, Flat bands as a route to high-temperature superconductivity in graphite, in *Basic Physics of Functionalized Graphite*, edited by P. D. Esquinazi (Springer, Cham, 2016), pp. 123–143.

[48] A. Y. Kitaev, Unpaired Majorana fermions in quantum wires, Phys. Usp. **44**, 131 (2001).

[49] See Supplemental Material at http://link.aps.org/supplemental/10.1103/PhysRevB.104.L060401 for detailed analytical calculations.

[50] H. Kondo, Y. Akagi, and H. Katsura, $\mathbb{Z}_2$ topological invariant for magnon spin Hall systems, Phys. Rev. B **99**, 041110(R) (2019).

[51] H. Kondo, Y. Akagi, and H. Katsura, Non-Hermiticity and topological invariants of magnon Bogoliubov–de Gennes systems, Prog. Theor. Exp. Phys. **2020**, 12A104 (2020).

[52] R. Resta, Macroscopic polarization in crystalline dielectrics: The geometric phase approach, Rev. Mod. Phys. **66**, 899 (1994).

[53] W. A. Benalcazar, B. A. Bernevig, and T. L. Hughes, Quantized electric multipole insulators, Science **357**, 61 (2017).

[54] M. Lin and T. L. Hughes, Topological quadrupolar semimetals, Phys. Rev. B **98**, 241103(R) (2018).

[55] J. Liu, M. Shi, J. Lu, and M. P. Anantram, Analysis of electrical-field-dependent Dzyaloshinskii-Moriya interaction and magnetocrystalline anisotropy in a two-dimensional ferromagnetic monolayer, Phys. Rev. B **97**, 054416 (2018).

[56] T. Srivastava, M. Schott, R. Juge, V. Křižáková, M. Belmeguenai, Y. Roussigné, A. Bernand-Mantel, L. Ranno, S. Pizzini, S.-M. Chérif, A. Stashkevich, S. Auffret, O. Boulle, G. Gaudin, M. Chshiev, C. Baraduc, and H. Béa, Large-voltage tuning of Dzyaloshinskii–Moriya interactions: A route toward dynamic control of skyrmion chirality, Nano Lett. **18**, 4871 (2018).

[57] W. Zhang, H. Zhong, R. Zang, Y. Zhang, S. Yu, G. Han, G. L. Liu, S. S. Yan, S. Kang, and L. M. Mei,

Electrical field enhanced interfacial Dzyaloshinskii-Moriya interaction in MgO/Fe/Pt system, Appl. Phys. Lett. **113**, 122406 (2018).

[58] H. Takagi, T. Takayama, G. Jackeli, G. Khaliullin, and S. E. Nagler, Concept and realization of Kitaev quantum spin liquids, Nat. Rev. Phys. **1**, 264 (2019).

[59] S. K. Choi, R. Coldea, A. N. Kolmogorov, T. Lancaster, I. I. Mazin, S. J. Blundell, P. G. Radaelli, Y. Singh, P. Gegenwart, K. R. Choi, S.-W. Cheong, P. J. Baker, C. Stock, and J. Taylor, Spin Waves and Revised Crystal Structure of Honeycomb Iridate Na_2IrO_3, Phys. Rev. Lett. **108**, 127204 (2012).

[60] S. Lee, S. Choi, J. Kim, H. Sim, C. Won, S. Lee, S. A. Kim, N. Hur, and J.-G. Park, Antiferromagnetic ordering in Li_2MnO_3 single crystals with a two-dimensional honeycomb lattice, J. Phys.: Condens. Matter **24**, 456004 (2012).

[61] P. Strobel and B. Lambert-Andron, Crystallographic and magnetic structure of Li_2MnO_3, J. Solid State Chem. **75**, 90 (1988).

[62] Y. Takahashi, N. Kijima, H. Hayakawa, J. Awaka, and J. Akimoto, Single-crystal synthesis and structure refinement of Li_2MoO_3, J. Phys. Chem. Solids **69**, 1518 (2008).

[63] S. Toth and B. Lake, Linear spin wave theory for single-q incommensurate magnetic structures, J. Phys.: Condens. Matter **27**, 166002 (2015).